# Micro computed tomography and CFD simulation of drop deposition on gas diffusion layers



2014 J. Phys.: Conf. Ser. 547 012028

(http://iopscience.iop.org/1742-6596/547/1/012028)

Journal of Physics: Conference Series **547** (2014) 012028 doi:10.1088/1742-6596/547/1/012028

# Micro computed tomography and CFD simulation of drop deposition on gas diffusion layers

**M Guilizzoni[1], M Santini[2], M Lorenzi[3], V Knisel, S Fest-Santini[2]**

[1] Dipartimento di Energia, Politecnico di Milano, via Lambruschini 4, 20156 Milano
[2] Dipartimento di Ingegneria, Università di Bergamo, viale Marconi 5, 24044 Dalmine (BG)
[3] School of Engineering and Mathematical Sciences, City University London, Northampton Square, London EC1V 0HB, UK

E-mail: maurizio.santini@unibg.it

**Abstract**. Fuel cells are electrochemical power generation system which may achieve high energy efficiencies with environmentally friendly emissions. Among the different types, Proton Exchange Membrane fuel cells (PEMFC) seem at present one of the most promising choices. A very important component of a PEMFC is the gas diffusion layer (GDL), which has the primary role of managing water in the cell, allowing reactant gases transport to the catalyst layer while keeping the membrane correctly hydrated and preventing electrode flooding. Therefore, GDLs have to be porous and very hydrophobic. Carbon clothes or carbon papers coated with a hydrophobizing agent – typically a fluoropolymer – are used. Given the complex chemistry and morphology of the GDLs, wettability analyses on them present some critical issues when using the conventional contact angle measurement techniques. In this paper, the deposition of a drop on a GDL (produced using polytetrafluoroethylene-co-perfluoroalcoxy vinyl ether as the fluorinated polymer) was investigated by means of micro computed tomography (microCT) and numerical simulation. The microCT facility operational at the University of Bergamo was used to acquire a 3D tomography of a water drop deposed on a sample GDL. The reconstructed drop dataset allows thorough understanding of the real drop shape, of its contact area and contact line. The GDL dataset was used to create a realistic mesh for the numerical simulation of the drop deposition, which was performed using the OpenFOAM® *interFOAM* solver.

## 1. Introduction

Fuel cells are electrochemical power generation systems where chemical energy is directly converted into electrical energy, without passing through combustion [1,2]. Their high energy efficiencies and environmentally friendly emissions make them very promising, even if a series of issues still has to be solved before their large scale application might be feasible. They also constitute a highly interesting topic from the theoretical point of view, as their design involves chemical, electrical, mechanical, thermal and fluid dynamic aspects at both the macro- and the microscale. Therefore, they constitute a field of very active research. Among the different available types of fuel cell, Proton Exchange Membrane fuel cells (PEM-FC) work at low temperatures with hydrogen as fuel, offering high power densities and flexibility to load changes. A fundamental component in a PEMFC (and also in other types, e.g. microbial fuel cells [3]) is the Gas Diffusion Layers (GDL). One of the major tasks for a GDL is to manage water within the cell [4], acting as a barrier to water transport – thus maintaining

the electrolyte membrane correctly hydrated and keeping the ionic conductivity high – and letting water pass only through some of the pores, keeping the most of the pores free for the reactants fluxes. To carry out such task, it has to be porous and highly hydrophobic. GDLs are therefore made of carbon fibers hydrophobized by a fluoropolymer dispersed on them. The fibers may be arranged either as a proper carbon fabric with a real warp-and-weft structure (carbon cloth) or in a woven-non-woven texture (carbon papers) obtained by high temperature sintering. The most used hydrophobizing agent is PTFE, but other fluoropolymers are under study too, e.g. perfluoroalcoxy (PFA), fluorinated ethylene propylene (FEP), fluorinated polyurethane based on perfluoropolyether (PFPE) blocks [5].

The high importance of the GDL hydrophobicity for the fuel cell performance is matched by the complexity of its evaluation. GDLs are absolutely far from the ideal surfaces on which the Young equation [6] and the conventional contact angle measurement techniques can be easily applied. They are chemically inhomogeneous, not flat, with a multi-scale roughness (from the fiber roughness to the warp-and-weft texture) which is only pseudo-isotropic. Moreover, they have to be extremely hydrophobic, up to the limit of superhydrophobicity (contact angle $\geq 150°$, contact angle hysteresis $\leq 10°$). All these conditions pose very significant difficulties [7] also to the state-of-the-art techniques for wettability analysis using sessile drops (which is the most commonly used method), e.g. Axisymmetric Drop Shape Analysis (ADSA) [8]. The major issues are that on such surfaces:

- the contact angle may be, and in general is, different from point to point along the triple line due to the surface morphology and to the triple line pinning on the surface edges [9];
- the apparent contact angle, i.e. the angle that the drop contour forms with an ideal horizontal line cutting the base surface at the contact points, is the only one accessible to conventional measurements (based on optical side-views acquisitions). The apparent contact angle may be related to the real contact angle by means of different models, among which the most credited are still the Wenzel model [10] – for homogeneous surfaces in which the drop liquid completely fills the grooves in the surface texture – and the Cassie-Baxter model [11], to be used for chemically heterogeneous surfaces or when the drop does not fill the grooves. The effectiveness of such models for surfaces characterized by multivariate wetting scenarios is still debated in the literature, so that detailed experiments about chemically and morphologically complex surfaces are needed for their validation;
- when conventional optics are used, the measurement may be affected by lens distortion, small depth of field with focus problems (particularly for the identification of the baseline), low or excess lighting or non-parallel light direction, low resolution of the image, diffraction near the contact points (particularly for very high contact angles). Moreover, side views of the drop-surface system may not be equivalent to real cross sections of the same;

Thus, there is a need to develop new techniques to improve the contact angle measurement and more in general the wettability analysis (triple line, wetted area, adhesion) of complex surfaces. GDLs are excellent test surfaces, as they join complexity and usefulness for practical applications.

In this work the use of micro computed tomography (microCT) is proposed to acquire a real three-dimensional representation of a sessile drop on a GDL surface, with the aim of extracting from the tomographic volume both direct experimental information about the drop shape and the surface wettability, and a realistic mesh for the numerical simulation of a drop deposition onto such surfaces.

## 2. Micro computed tomography

Among several emerging tomographic imaging techniques (derived using different physical phenomena, e.g. gamma rays, radio-frequency waves, electrical resistance, electrons, magnetic particles) currently available for the non-invasive visualization of the inside of an opaque material, the microCT is the one with highest spatial resolution and good penetrating capability. Thus, it is the most suited non-destructive technique (NDT) for the morphological reconstruction of multiphase interfaces at microscale.

A prototype microCT set-up (Fig. 1) is operational at the University of Bergamo composed by a X-ray microfocus open type emission tube (160 kVp @ 200 microA) allowing the emission as Bremsstrahlung (i.e. polychromatic and incoherent) with energies ranges suitable for micrometric

spatial resolution tomography in a millimetric size sample. Projections are acquired by digital detectors (CCD flat panels with optimized scintillators are used to capture X-ray intensity). A rotary air-bearing direct drive stage provides superior angular positioning. The object itself is placed on the stage and rotated by angular steps according to Nyquist-Shannon theorem. Volumes are reconstructed with filtered back-projection standard algorithm, using commercial software VGStudio MAX, generating a 3D digital image of the object.

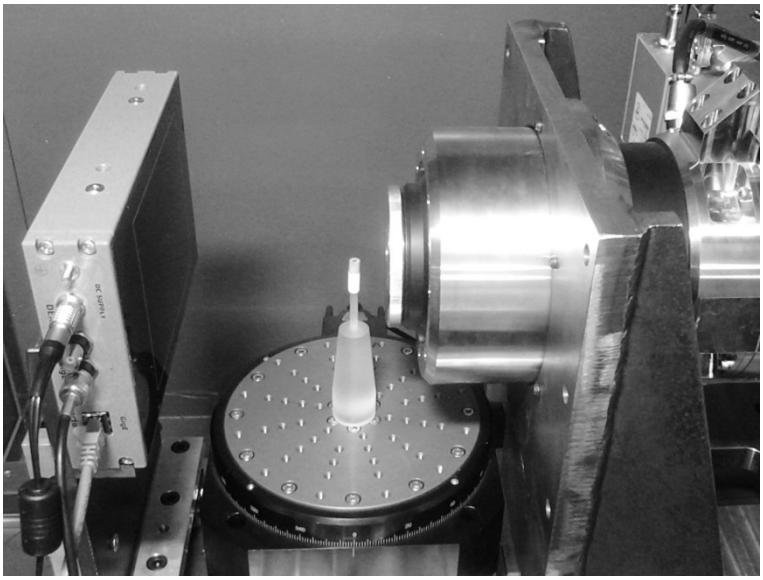

**Figure 1**. microCT set-up at the University of Bergamo.

## 3. Numerical simulations

Numerical simulations were performed using the *interFoam* solver of the OpenFOAM® 2.2.0 open source CFD toolbox [12]. OpenFOAM® was selected due to its free and open source nature and to the many favorable reviews and successful cases of application described in the literature [e.g. 13-17]. *interFoam* is a isothermal finite volume solver implementing a modified version of the Volume of Fluid (VOF) [18] method to simulate two-phase flow using a single set of equations. Both phases are assumed as incompressible and surface tension is included by means of the continuum surface force (CSF) model [19]. Volume tracking and interface reconstruction, with no explicit interface tracking, is performed. With respect to the original VOF formulation, the *interFoam* model includes an additional term in the volume fraction equation (Eqn. 1), to obtain interface compression down to just 2-4 cells. The full set of the governing equations solved by *interFoam* is thoroughly described in [13,14,17]. In summary, it is constituted by the incompressible continuity and Navier-Stokes equation system, plus an equation for the transport of the volume fraction (also called color function) $\alpha$:

$$\frac{\partial \alpha}{\partial t} + \nabla \cdot (\mathbf{u}\,\alpha) + \nabla \cdot [\mathbf{u_r}\,\alpha(1-\alpha)] = 0 \tag{1}$$

In the last equation, $u_r$ is the so-called "compression velocity" that performs interface compression. In strict terms, such an additional term is a mass source, but both literature results [17] and verification by the authors proved that mass variation is completely negligible.

The drop water and the surrounding air were both assumed as Newtonian fluids, and the flow as laminar. For each phase the values of all the relevant thermophysical properties were taken at ambient temperature (20 °C). The drop diameter and the initial position of the drop with respect to the solid

substrate were fixed using the *setFields* OpenFOAM® utility, assuming an initially spherical and still drop.

Previous tests by the authors [20] confirmed that the discretization schemes (both for space and time), solution algorithms and solver settings indicated in [17] are the most suitable for the investigated cases. Automatic time step adaptation was used to keep the Courant–Friedrichs–Lewy (CFL) number under the limit of 0.3 which is requested by the peculiar interface compression scheme used in *interFoam* for 3D simulations [13]. Some volume fraction sub-cycles were also performed to further improve the accuracy. The side effect of these choices is obviously that for the very fine meshes required by the GDL structure such a low value of the CFL number implies very small time steps and consequently very long simulation times.

Both complete 3D simulations and 2D simulations on single slices of the investigated volume were performed. For the 3D simulations, the domain was modeled as a "box" having sides of a few millimeters and whose bottom is constituted by the real GDL surface. The latter was extracted from the tomographic volume as an isosurface at the proper intensity value and exported as a stereolithography (STL) file. A structured mesh was initially created filling a box with regular hexaedra and then the OpenFOAM® *snappyHexMesh* utility was used to modify such basic mesh. For 2D simulations, a completely analogous procedure was followed, with the only difference that an extrusion of the selected volume slice was used as the bottom of the domain.

*snappyHexMesh* is able to perform different steps in mesh processing:

- select, from the base mesh, only the cells which are on one side of the surface described by the STL file; this creates a mesh with jagged boundaries;
- snap the vertices of the selected cells to their nearest points on the surface, so that the resulting mesh boundaries follows the original limiting surface;
- add boundary layer cells, if desired to better capture boundary layer phenomena.

For this work, only the first two steps were performed. In Fig. 2 examples of the resulting mesh after the first step and after the second are presented, both for 3D (top row) and 2D (bottom row) domains. The zooms from the 2D meshes are shown to better evidence the effect of the snapping step. Regrettably, the GDL surface is extremely complex, so that the snapping step creates a mesh that may include a certain number of extremely small and skewed cells, particularly in 3D. Great care has therefore to be devoted to obtaining a correct mesh, and in any case the CFL number limit requires time steps so small that 3D simulations become unfeasible on common personal computers. Therefore, the simulations described in this work were run on the snapped mesh in 2D, while using the jagged meshes in 3D. The use of jagged meshes worsens the well-known issues about contact angle and surface tension modeling – common to all non-smoothed interface-tracking and interface-reconstruction algorithms – that result in the development of spurious velocities near the interface. On small domains, the latter may heavily affect the reliability of the simulation. This is a quite common situation for analysis concerning complex surfaces (e.g. for porous media) and suitable countermeasures are under development to overcome these issues [21]. They require significant modifications of the solvers, which were not taken on here. Moreover, the simulation time in 3D was very long (some weeks for each simulation), with the consequence that rigorous mesh independence studies could not be carried out on 3D simulations. Therefore, they were performed on 2D simulations, while only preliminary checks about mesh independence were performed in 3D. Table 1 reports the domain and mesh characteristics for the performed simulations, while Fig. 3 shows the mesh dependence of the drop profile during the first part of the deposition in 2D simulations. It can be noticed how the drop profile and main drop dimensions are mesh independent. Concerning 3D simulations, no significant difference in the results were found with the finer mesh, apart from minor improvements in the resolution of the results and in the reduction of the spurious velocities.

The described issues concerning the mesh should be kept in mind in the evaluation of the simulation results, which at present must be considered mainly as a preliminary "feasibility study" about this topic, to trace the route for more in-depth studies.

Concerning boundary conditions:

- the top and the side boundaries of the domain were set as open boundaries at fixed total pressure, with volume fraction equal to 1 for the air phase (the drop must not reach such boundaries during the interesting part of the simulation);
- the bottom (modeling the GDL surface) was set as a no-slip wall at fixed flux pressure, with a dynamic contact angle condition for the volume fraction. The latter b.c. is defined in OpenFOAM® on the basis of the maximum advancing and minimum receding contact angles, plus a scaling velocity which allows the calculation of the effective contact angle in dependence of the velocity of the interface in contact with the boundary.

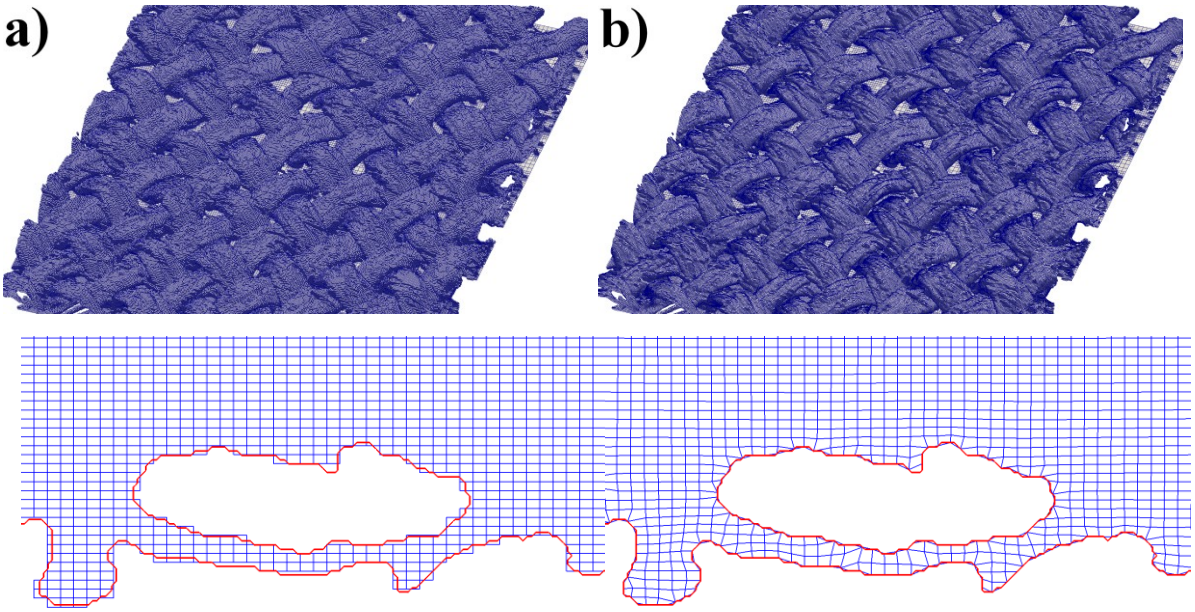


**Figure 2.** Mesh after running *snappyHexMesh* for the GDL-PFA cases: a) 3D case, cell selection alone, b) 3D case, cell selection and snapping to the limiting surface. On the bottom row, a zoom from the 2D intermediate mesh (see Tab. 1) is shown, to better evidence the effect of the snapping step (the limiting surface is drawn in red). (For interpretation of the references to color in this figure caption, the reader is referred to the Web version of this article.)

**Table 1.** Domain and mesh details for the performed simulations.

| | Domain dimensions [m] | Number of cells [kcell] |
|---|---|---|
| **GDL-PFA 2D coarse** | 0.0064 x 0.0042 | 37.17 |
| **GDL-PFA 2D intermediate** | 0.0064 x 0.0042 | 148.9 |
| **GDL-PFA 2D fine** | 0.0064 x 0.0042 | 595.6 |
| **GDL-PTFE 3D coarse** | 0.0040 x 0.0040 x 0.0020 | 1701 |
| **GDL-PTFE 3D fine** | 0.0030 x 0.0030 x 0.0020 | 4100 |
| **GDL-PFA 3D** | 0.0040 x 0.0040 x 0.0040 | 3916 |

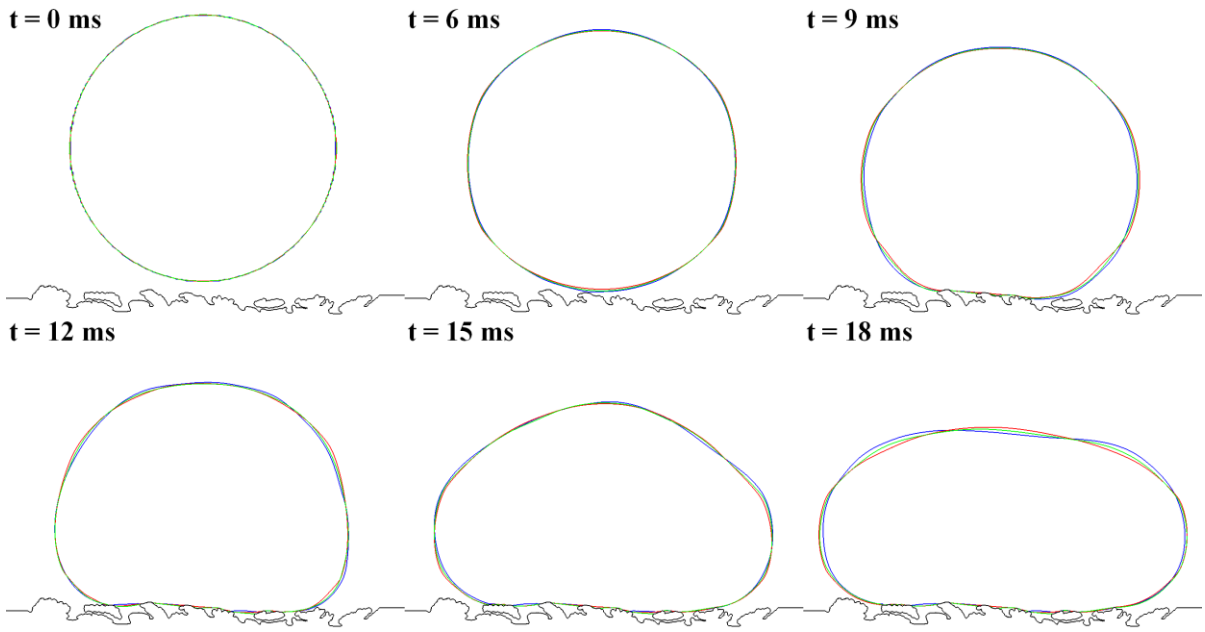


**Figure 3**. Mesh dependence of the drop profile during the first part of the deposition in 2D simulations: cases GDL-PFA 2D coarse (blue), GDL-PFA 2D intermediate (green), GDL-PFA 2D fine (red). (For interpretation of the references to color in this figure caption, the reader is referred to the Web version of this article.)

## 4. Results

As test surfaces, two GDLs – prepared by the Materials for Energy and Environment group of the Chemistry, Materials and Chemical Engineering Department of Politecnico di Milano – were used. The carbon matrix is the same for both, but one was hydrophobized using PTFE and the other using PFA. The voxel resolutions of the tomographic scans are 8 μm and 5.12 μm for the GDL-PTFE and GDL-PFA surfaces, respectively. Figures 4 a) and b) show the isosurface extracted from the tomographic volume for the two GDLs. As already described, such isosurfaces were saved as STL files and used to prepare the mesh for the numerical simulations.

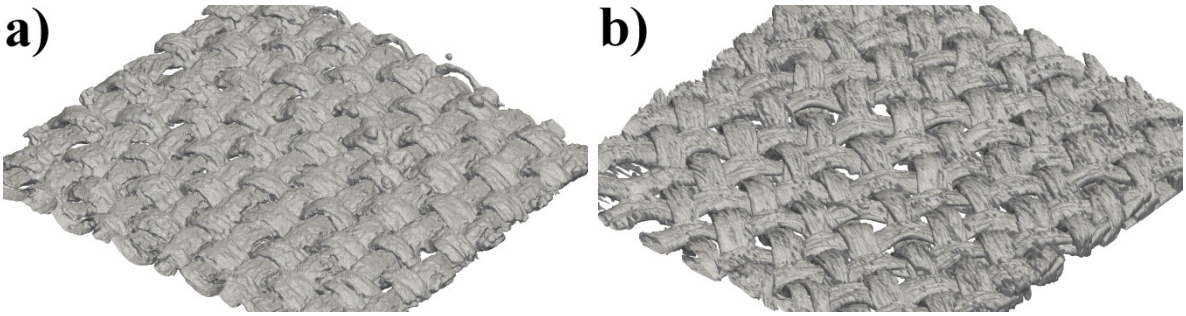


**Figure 4.** GDL-PTFE (a) and the GDL-PFA (b) surfaces extracted as intensity isosurfaces from the tomographic volume.

The GDL-PFA was also acquired after a drop was deposed on it. Figures 5 a) and b) show such situation both by means of a conventional side view taken with a SLR camera with macro lens and as the isosurfaces for drop and GDL after tomographic acquisition. It is evident how the tomographic reconstruction offers a much higher level of detail, with a micrometric resolution which is unreachable

by the conventional optical investigation techniques and in a real three-dimensional reconstructed volume, which cannot be obtained with conventional electron microscopy.

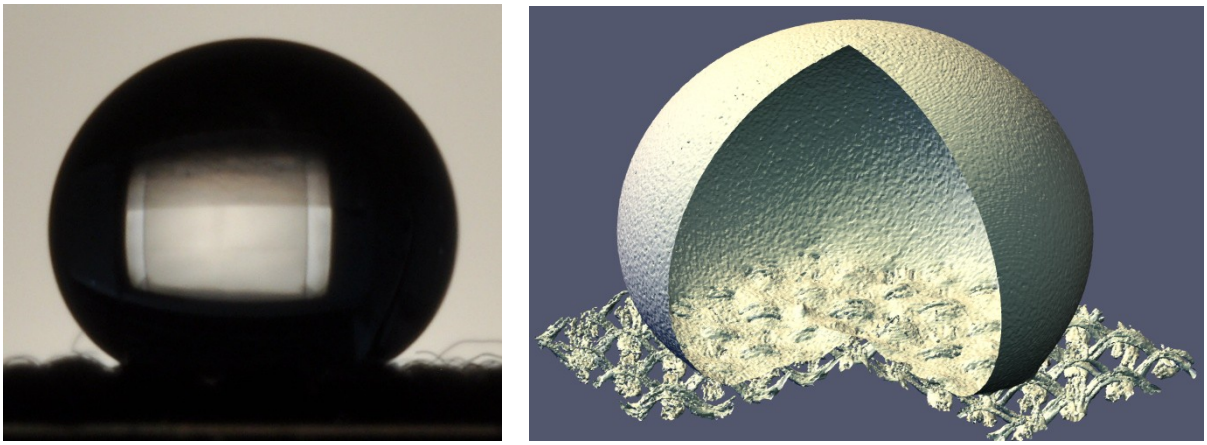

**Figure 5.** Optical side view of a sessile drop deposed on a GDL-PFA surface (left) and drop and GDL surfaces extracted from the reconstructed tomographic volume (right).

The tomographic output can be further processed to get accurate measurements of the drop volume and surface area, of the wetted area and of the real shape of the contact line [22,23]. It can also be sliced both horizontally, to get information about the water permeation within the GDL fibers (Fig. 6), and vertically, to evidence the complexity of the wetting, e.g. with pinning on the fibers (Fig. 7). If polar vertical slices are extracted and the drop is assumed to be macroscopically axisymmetric, axisymmetric drop shape analysis (ADSA) can also be applied to get information about the contact angle on a slice-wise basis [22]. Using such an approach, the average contact angle on the GDL-PFA was calculated and compared with the measurement by conventional ADSA on sessile drop pictures. Good agreement was obtained between the two approaches, with an average value of the "as placed" static contact angle $\theta = 151°$ (std. dev. 0.6°) for the conventional measurements and $\theta = 154°$ (std. dev. 2.6°) for the microCT analysis. The higher standard deviation for the microCT case reflects the variability of the contact angle along the triple line, which can be easily missed when using the conventional approach. Dynamic contact angle measurements by the conventional approach evidenced a very low hysteresis.

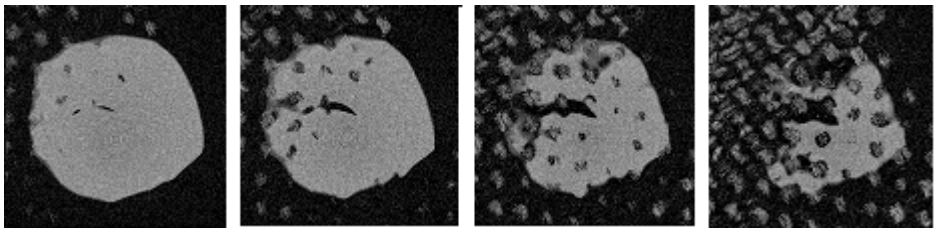

**Figure 6.** Horizontal slices of the tomographic volume for the GDL-PFA in the region where the drop wets the surface. Water volume included in each slice is 0.0518 μl, 0.0452 μl, 0.0315 μl, 0.0174 μl respectively.

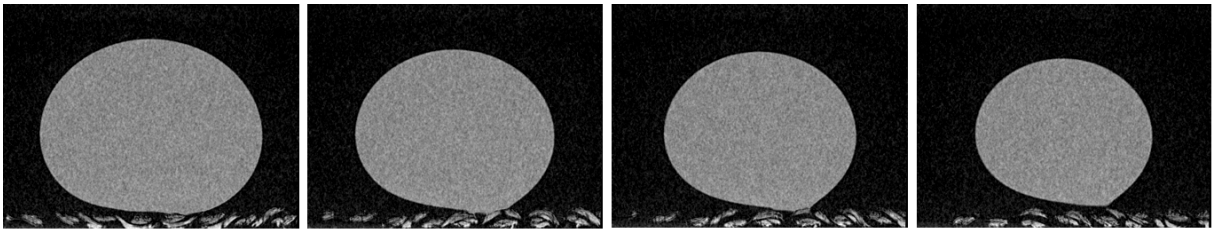

**Figure 7.** Vertical slices of the tomographic volume for the GDL-PFA, evidencing the complexity of the wetting with pinning on the fibers.

Therefore, a value of the static contact angle equal to 150° and a hysteresis of 10° were used as input for the simulation of the drop deposition on the GDL-PFA surface. On the contrary, a contact angle equal to 110° with and hysteresis of 20° – reflecting literature values for smooth PTFE – was arbitrarily set for the simulation on the GDL-PTFE surface, to simulate a less hydrophobic scenario. It is worth noting that the real wettability of GDL-PTFE is extremely similar to the one on the GDL-PFA, due to the dominating effect of morphology. Figure 8 shows some images of the drop shape during the deposition on the two surfaces. Figure 9 shows the time evolution of the apparent spreading ratio during the simulated deposition on the GDL-PTFE (case 3D fine). The apparent spreading ratio is defined here as the ratio between the wetted area vertically projected onto a horizontal plane and the equatorial section area of the drop before impact.

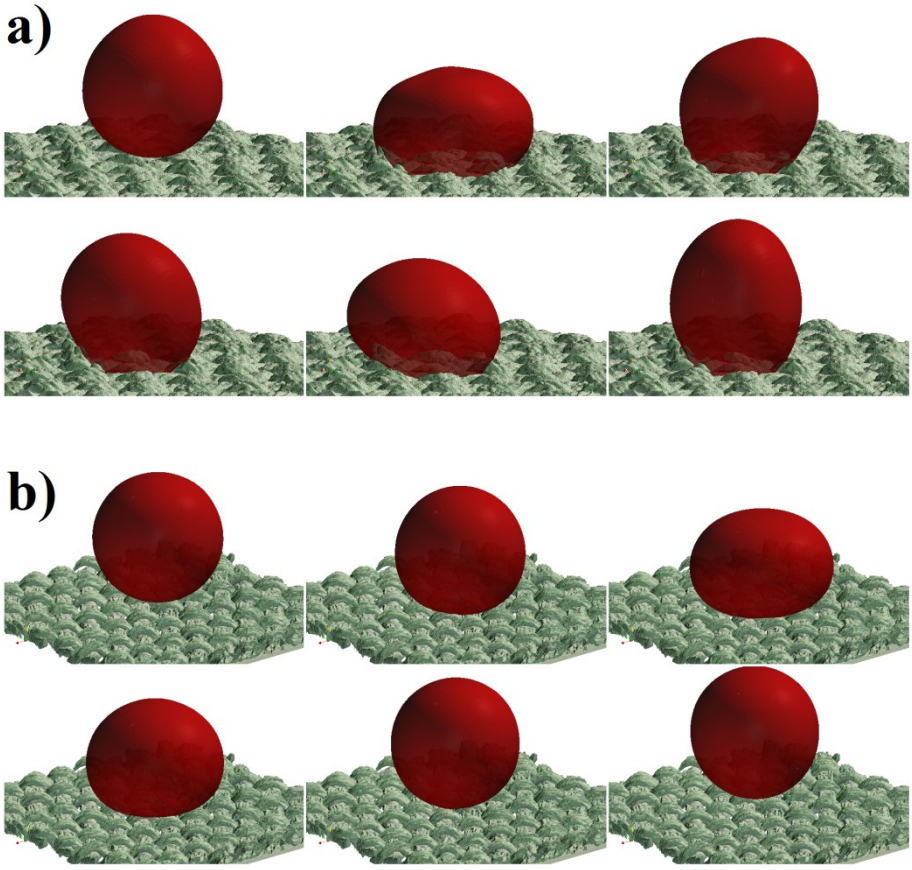


**Figure 8.** Drop shape during the first instants of the simulated deposition on the two investigated surfaces: GDL-PTFE (a) and GDL-PFA (b). The time step between the images is 2 ms.

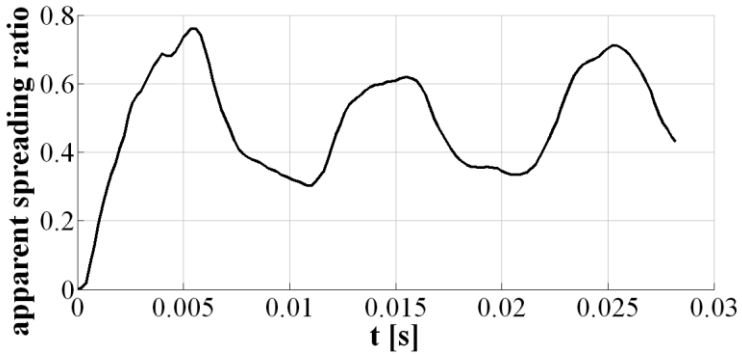


**Figure 9.** Apparent spreading ratio during simulated drop deposition on the GDL-PTFE.

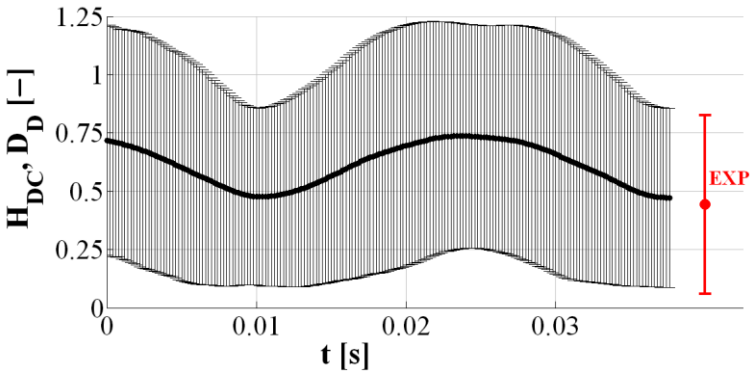


**Figure 10.** Normalized height ($H_{DC}$) of the drop center of mass and vertical drop diameter ($D_D$, shown by means of the error bars) during simulated drop deposition on the GDL-PFA. The equilibrium values for the corresponding experimental drop are represented in red on the right of the chart. (For interpretation of the references to color in this figure caption, the reader is referred to the Web version of this article.)

The drop on such less hydrophobic surface has a much wider wetted area and it remains pinned to the surface after the contact, while on the more hydrophobic surface the drop bounces back, despite the extremely low "impact" velocity. Figure 10 shows the time evolution of the normalized (with respect to the drop diameter before impact) height of the drop center of mass and drop vertical diameter during simulation on GDL-PFA (case 3D). The first was calculated from the reference plane identified by the lowest point of the GDL surface. The drop normalized diameter is shown in the figure by means of the error bars. The equilibrium values of such quantities for the experimental drop on the GDL-PFA substrate are also shown in red in the chart for comparison. The bouncing and deformation of the drop after impact is clearly evidenced and it is qualitatively consistent with direct observation during real drop deposition, even if the bouncing height in the simulations appears (no rigorous quantitative measurement was performed during the experimental part) excessive.

Concerning the final drop shape, the spurious velocities induce distortions and oscillations of the drop surface for a time which is much longer than the experimentally observed one. As a consequence, the condition of static equilibrium for the drops on the surfaces could only be reached in 2D simulations, which are obviously much faster, and thanks to a "trick": once the deposition dynamics of interests were captured, the viscosities of the phases were increased 1000 times to reduce the spurious velocities and dampen the oscillations (as in [24]). In fact, viscosity for Newtonian fluids has no influence on the drop equilibrium shape, which is only related to the capillary constant and curvature radii at the drop apex. Thus the ADSA technique to evaluate the drop shape and contact angle from vertical slices of the simulated drops could be applied. The contact angle in this case is a trivial result:

being one of the boundary condition of the simulation, it is obviously reproduced. On the contrary, analysis of the drop shape is a good validation of the simulation performances. Vertical slices of the simulated volume (Fig. 11, right part) show that on the more hydrophobic surface the drop is in a Cassie-Baxter wetting state, with air pockets entrapped between the drop and the GDL. This is consistent with the experimental evidence from microtomographic scans (Fig. 11, left part). Table 2 summarizes the results of ADSA analysis on the tomographic slices and on the results of the 2D simulation for GDL-PFA, while Fig. 12 provide an example of the fitted theoretical drop contours on the slices (experimental and numerical) shown in Fig. 11.

**Table 2.** ADSA results for experimental and simulated drops.

| | **Experimental drop** | **Simulated drop (2D)** |
|---|---|---|
| **Estimated drop volume** (real value directly obtained by microtomography: 40.945 µl) | 40.960 µl | 41.429 µl |
| **Eötvös number** | 0.919 | 0.946 |
| **Height over maximum diameter ratio** | 0.709 | 0.714 |
| **Curvature radius at the drop apex** | 2.60 mm | 2.64 mm |

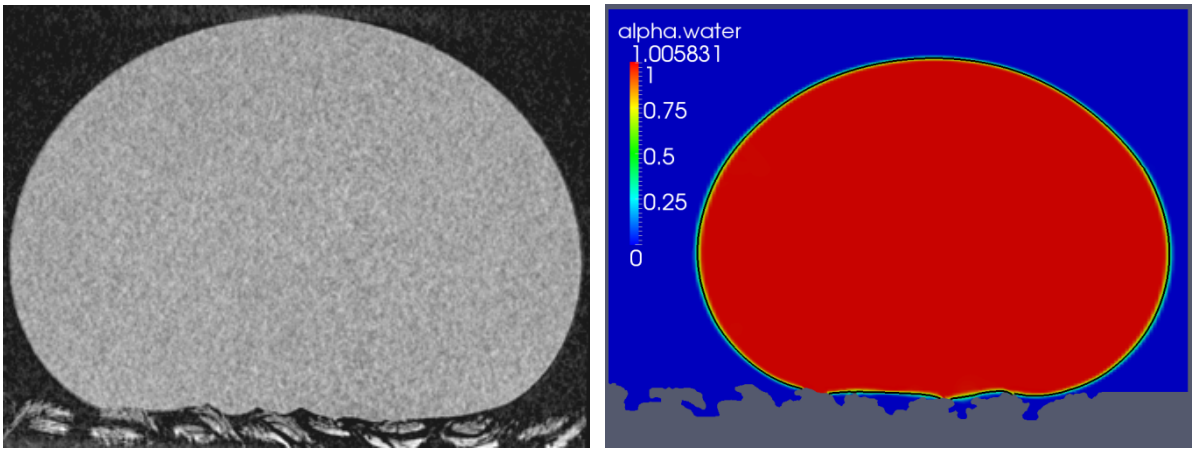


**Figure 11.** Vertical slices of the domain in correspondence of the drop apex, evidencing the Cassie-Baxter wetting state, for the tomographic (left) and simulated (right, color scale proportional to the water volume fraction) cases on GDL-PFA.

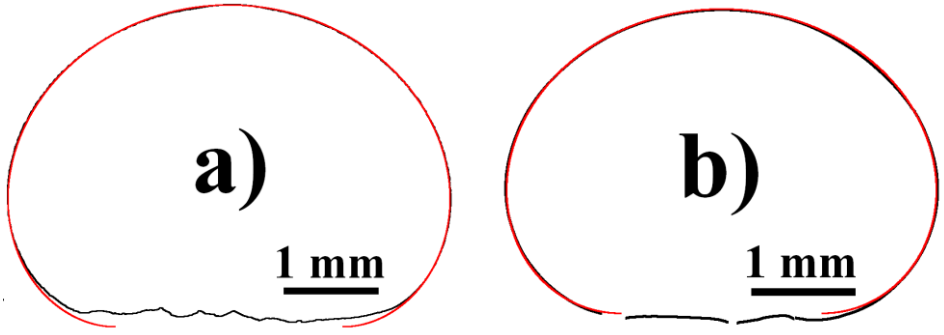


**Figure 12.** Theoretical drop profile from ADSA analysis (red) superposed to the drop contour (black) extracted from a tomographic slice (a) and 2D simulation (b). Contours have been enlarged for better visualization and the scale factor is slightly different between the two images. (For interpretation of the references to color in this figure caption, the reader is referred to the Web version of this article.)

It is evident how both drop profiles can be satisfactorily fitted with the numerical integration of the Laplace-Young equation, apart from the contact region where the drop pinning on the GDL fibers alters the drop shape with respect to the theoretical one (which is developed for a perfectly smooth surface). The curvature radius at the apex, the height over maximum diameter ratio, the Eötvös number are well reproduced by the simulation.

## 5. Conclusions

Computer-aided microtomography (microCT) was used to investigate wettability for two gas diffusion layers for fuel cells, both of cloth type but hydrophobized using different fluoropolimers (PTFE and PFA). Such surfaces pose high difficulties for conventional wettability studies. A sessile drop deposed on the GDL-PFA surface was acquired by the microCT and information about the real contact area, contact line and contact angle could be obtained from the tomographic volume. The microCT scan also allows direct visualization of the contact region, confirming that on the highly hydrophobic and morphologically complex GDL structure the drop is in a Cassie-Baxter wetting state. The two GDL surfaces extracted from the tomographic volume were then used to create a realistic mesh for the numerical simulation of drop deposition on such surfaces, using the VOF technique. The complexity of the resulting mesh is a serious issue for the reliability of the simulations, particularly due to spurious velocities and dynamic contact angle modeling. Nevertheless, simulation results were consistent both qualitatively and partially quantitatively with experimental observations.

## Acknowledgments

The financial support from the Regione Lombardia (Italy) within the call “Cooperazione Scientifica e Tecnologica Internazionale nelle aree tematiche agroalimentare, energia-ambiente, salute e manifatturiero avanzato” Project ID-MAN11 and the research fund grant to Maurizio Santini “Fondi di Ricerca di Ateneo” and also the prize “5 per 1000” of the University of Bergamo (Italy) are gratefully acknowledged. The research Grant of Stephanie Fest-Santini was financed within “Progetto ITALY® – Azione Giovani in Ricerca anno 2013” of the University of Bergamo (Italy).

## References

[1] Barbir F 2005 *PEM fuel cells: theory and practice* (Amsterdam: Elsevier Academic Press)
[2] Wee J, 2007 Applications of proton exchange membrane fuel cell systems *Renew Sustain Energy Rev* **11** 1720–38
[3] Santoro C, Guilizzoni M, Correa Baena J P, Pasaogullari U, Casalegno A, Li B, Babanova S., Artyushkova K and Atanassov P 2014 The effects of carbon electrode surface properties on bacteria attachment and start up time of microbial fuel cells *Carbon* **67** 128–39
[4] Dai W, Wang H, Yuan X-Z, Martin J J, Yang D, Qiao J and Ma J 2009 A review on water balance in the membrane electrode assembly of proton exchange membrane fuel cells *Int J Hydrogen Energy* **34** 9461–78
[5] Latorrata S, Balzarotti R, Gallo Stampino P, Cristiani C, Dotelli G and Guilizzoni M, 2014, Design of properties and performances of innovative gas diffusion media for polymer electrolyte membrane fuel cells, *Progress in Organic Coatings*, in press
[6] Young T 1805 An essay on the cohesion of fluids *Philos Trans R Soc Lond* **95** 65–87
[7] Extrand C W, Moon S I 2010 Contact Angles of Liquid Drops on Super Hydrophobic Surfaces: Understanding the Role of Flattening of Drops by Gravity *Langmuir* **26(22)** 17090–99

[8] del Río O I, Neumann A W 1997 Axisymmetric Drop Shape Analysis: Computational Methods for the Measurement of Interfacial Properties from the Shape and Dimensions of Pendant and Sessile Drops *J. Colloid and Interface Sci* **196(2)** 136–47
[9] Tadmor R 2004 Line Energy and the Relation between Advancing, Receding, and Young Contact Angles *Langmuir* **20** 7659–64
[10] Wenzel R N 1936 Resistance of solid surfaces to wetting by water *Ind. Eng. Chem.* **28** 988–94
[11] Cassie A B D, Baxter S 1944 Wettability of porous surfaces *Trans. Faraday Soc.* **40** 546–51
[12] OpenFOAM®, The open source CFD toolbox, 2013. <http://www.openfoam.com/> (accessed October 2013)
[13] Gopala V R, van Wachem B G M 2008 Volume of fluid methods for immiscible-fluid and free-surface flows *Chemical Engineering Journal* **141** 204–21
[14] Deshpande S, Anumolu L and Trujillo M F 2012 Evaluating the performance of the two-phase flow solver interFoam *Computational Science & Discovery* **5** 014016 1–37
[15] Berberovic E, van Hinsberg N P, Jakirlic S, Roisman I V and Tropea C 2009 Drop impact onto a liquid layer of finite thickness: Dynamics of the cavity evolution *Physical Review E* **79** 036306
[16] Trujillo M F, Lewis S R 2012 Thermal boundary layer analysis corresponding to droplet train impingement *Physics of Fluids* **24** 112102 1–23
[17] Deshpande S, Trujillo M F, Wu X and Chahine G 2012 Computational and experimental characterization of a liquid jet plunging into a quiescent pool at shallow inclination *Int. J. Heat and Fluid Flow* **34** 1–14
[18] Hirt C W, Nichols B D 1981 Volume of Fluid (VOF) Method for the Dynamics of Free Boundaries *J. Computational Physics* **39(1)** 201–225
[19] Brackbill J U, Khote D B and Zemach C 1992 A Continuum Method for Modeling Surface Tension *J. Computational Physics* **100** 335–354
[20] Fest-Santini S, Guilizzoni M, Santini M and Cossali G E 2012 Water drop impact into a deep pool: influence of the liquid pool temperature, Proceedings of the Droplet Impact Phenomena & Spray Investigations (DIPSI) Workshop 2012, Dalmine (Italy), http://aisberg.unibg.it/handle/10446/27138
[21] Raeini A Q, Blunt M J and Bijeljic B 2012 Modelling two-phase flow in porous media at the pore scale using the volume-of-fluid method *J. Computational Physics* **231** 5653–68
[22] Santini M, Guilizzoni M and Fest-Santini S 2013 X-ray computed microtomography for drop shape analysis and contact angle measurement *J. Colloid and Interface Sci.* **409** 204–210
[23] Santini M, Guilizzoni M 2014 3D X-ray micro computed tomography on multiphase drop interfaces: from biomimetic to functional applications *Colloid and Interface Sci. Comm.* **1** 14–17
[24] Guilizzoni M 2011 Drop shape visualization and contact angle measurement on curved surfaces *J. Colloid and Interface Sci.* **364** 230–236